chemosensors

Article

Spectroscopic Recognition of Metal Ions and Non-Linear Optical (NLO) Properties of Some Fluorinated Poly(1,3,4-Oxadiazole-Ether)s

Mihaela Homocianu *, Anton Airinei, Alina Mirela Ipate and Corneliu Hamciuc

"Petru Poni" Institute of Macromolecular Chemistry, 41A, Grigore Ghica Voda Alley, 700487 Iasi, Romania; airineia@icmpp.ro (A.A.); ipate.alina@icmpp.ro (A.M.I.); chamciuc@icmpp.ro (C.H.)
* Correspondence: michalupu@yahoo.co.uk or mlupu@icmpp.ro; Tel.: +0232-217-454

Abstract: In this paper, we examined the sensing ability of some fluorinated 1,3,4-oxadiazole-containing assemblies toward various metal ions and their nonlinear optical (NLO) properties. The changes in the spectral characteristics of these compounds in the existence of Mg^{2+}, Mn^{2+}, Ni^{2+}, Cd^{2+}, Zn^{2+}, Co^{2+}, Cu^{2+}, Hg^{2+}, Sn^{2+}, and Ag^{+} metal ions were performed, and they were found to be selective and more sensitive toward the addition of Ag^{+}, Co^{2+}, and Cu^{2+} ions (new bands appeared). Instead, spectral changes in the presence of Mg^{2+}, Mn^{2+}, Ni^{2+}, Cd^{2+}, Zn^{2+}, Hg^{2+}, and Sn^{2+} were not significant, so we did not evaluate the corresponding binding parameters. Therefore, all of these compounds were found to be selective and sensitive to Ag^{+}, Co^{2+}, and Cu^{2+} ions. Furthermore, the first-order polarizability (α_{CT}), the first-order hyperpolarizability (β_{CT}), and the second-order hyperpolarizability (γ_{CT}) were evaluated using the solvatochromic approach, and the intramolecular charge transfer (ICT) characteristics were investigated using a generalized Mulliken–Hush (GMH) analysis.

Keywords: fluorinated 1,3,4-oxadiazole assemblies; metal ion recognition; NLO properties; ICT characteristics

check for updates

Citation: Homocianu, M.; Airinei, A.; Ipate, A.M.; Hamciuc, C. Spectroscopic Recognition of Metal Ions and Non-Linear Optical (NLO) Properties of Some Fluorinated Poly(1,3,4-Oxadiazole-Ether)s. *Chemosensors* **2022**, *10*, 183. https://doi.org/10.3390/chemosensors10050183

Received: 1 April 2022
Accepted: 9 May 2022
Published: 11 May 2022

1. Introduction

Recently, due to advancing environmental pollution, the recognition of various metal ions has become a vital requirement in various fields of biotechnology, material science, and environmental protection. Due to their excellent characteristics, including remarkable photophysical features, good chemical stability, and the option to be simply functionalized with diverse chromophore units and/or chelating groups, 1,3,4-oxadiazole assemblies are optimal materials for the development of optical sensors [1]. Detailed analysis and efforts to develop sensitive sensors that are used to detect metal ions in different environments, such as silver (Ag^{+}), copper (Cu^{2+}), and cobalt (Co^{2+}) ions, are constantly changing due to their presence in the human body, the environmental media, and in biological systems [2–4]. Recent research suggests that silver, copper, and cobalt ions have a significant impact on human health through diseases that are induced by their excess, lack, and/or toxicity (silver ions: gastrointestinal diseases [5]; copper ion toxicity: Menkes [6] and Wilson [7] diseases; cobalt ions: Parkinson's [8] and Alzheimer's [9] diseases). In addition to these effects on human health, Co^{2+} ions are widely applied in industry and medicine, including corrosion-resistant alloys, Co_{60} for radiotherapy [10,11], and materials containing silver ions that are significant for various industrial fields have been extensively used as catalysts, electrodes [12], and antimicrobial agents [13]. Numerous techniques, including plasma mass spectrometry [14], flame atomic absorption spectrometry [15], potentiometric methods [16], fluorescence sensors [17,18], and electroanalytical sensors [19] have been developed and are commonly used for the detection of Co^{2+}, Cu^{2+}, and Ag^{+} metal ions in real samples. Instead, several advantages have been reported concerning the use of spectroscopic studies for various molecular assemblies to act as detection probes, including

a high degree of sensitivity and selectivity in identifying different analytes, the ability to recognize multiple metal ions in aqueous solutions, a simple setup, a low response time, and a low cost [20].

So far, various sensing molecular assemblies containing 1,3,4-oxadiazole units have been studied to identify various metal ions, including Ca^{2+} [21], Cd^{2+} [22], Ag^{+} [23], Hg^{2+} [24], Fe^{3+} [25], and Zn^{2+} [26], while a limited number of references have been made for interactions between **fluorinated 1,3,4-oxadiazole derivatives** and various metal ions. For example, 2-(2-hydroxyphenyl)-5-(4-methoxyphenyl)-1,3,4-oxadiazole was involved in the recognition of Zn^{2+} in water solutions and showed a high degree of selectivity and sensitivity [27].

Fluorochemosensors having an oxadiazole (bis(*N*,*N*-bis(2-pyridylmethyl)amine) bridge have also been reported in the literature and have shown "on–off" fluorescence switch characteristics and a high selectivity for Cu^{2+} that is related to a range of other ions [28,29]. Zheng et al. [30] reported 2,5-bis(pyridine-2-formamidophenyl)-1,3,4-oxadiazole derivatives that exhibited good responses in the recognition of Ag^{+} ions.

Furthermore, molecular structures having 1,3,4-oxadiazole and showing NLO properties have attracted considerable interest due to their applications in different technical fields, including medicine [31], organic light-emitting diodes (OLED) [32], solar cells [33,34], quantum computing, and optoelectronics [35,36]. The nonlinear optical effects in organic compounds are predominantly a result of their electronic structure, resulting in a fast nonlinear response compared to inorganic NLO materials [37,38].

In this paper, we investigate the ability of some fluorinated 1,3,4-oxadiazole derivatives to recognize metal ions (i.e., Mg^{2+}, Mn^{2+}, Ni^{2+}, Cd^{2+}, Zn^{2+}, Co^{2+}, Cu^{2+}, Hg^{2+}, Sn^{2+}, and Ag^{+}) using absorption and fluorometric titrations, as well as nonlinear optical properties in different media. We also studied the NLO parameters α_{CT}, β_{CT}, and γ_{CT}, of the **fluorinated 1,3,4-oxadiazole assemblies** in relation to their solvatochromic behavior. The Mulliken-Hush method is employed to study the intramolecular charge transfer (ICT) characteristics of the **BisFOx** derivative.

2. Materials and Methods

2.1. Materials

The investigated **fluorinated 1,3,4-oxadiazole assemblies**, **BisFOx**, **9FOx**, and **6Fox**, were obtained via the aromatic nucleophilic substitution reaction of 2,5-bis(p-fluorophenyl)-1,3,4-oxadiazole with fluorinated bisphenols, as previously reported in the literature [39]. The nucleophilic substitution reaction between an aryl halide and a phenoxide is the most common method of synthesizing poly(aryl-ether)s. The polycondensation reactions have been performed in NMP solvent, using anhydrous potassium carbonate as the catalyst, and were performed at elevated temperatures. The 1,3,4-oxadiazole units in these compounds act as an activating group that receives a negative charge and thus causes the activation energy to decrease for the displacement of the p-substituted fluorine group by a Meisenheimer complex, similar to other activating groups, including ketone or sulfone [39].

The molecular structure and purity of the obtained compounds were confirmed via the analysis of FTIR(FTIR spectrophotometer, Bruker Optik GmbH, Ettlingen, Germany) and 1H NMR (Bruker Avance Neo instrument (Bruker BioSpin, Rheinstetten, Germany) data (given in Supplementary Material). The obtained FTIR spectra of the **1,3,4-oxadiazole derivatives** were analyzed by defining the registered peaks corresponding to the groups (OH–, C–O, C–H). From the FTIR spectra for the **BisFOx** sample, the followed peaks (cm^{-1}) were identified: 3047 (aromatic C–H), 1601 (aromatic C=C), 1246 (aromatic ether linkage), 1150 (trifluoromethyl group), 1013, and 961 (oxadiazole ring) [29]. The spectra for the **6FOx** sample include the following peaks (in cm^{-1}) 3052 (aromatic C–H), 1603 (aromatic C=C), 1247 (aromatic ether linkage), 1173, 1210 (hexafluoroisopropylidene group), 1020, and 968 (oxadiazole ring) [39], and for **6FOx**, the following peaks: 3073 (aromatic C–H), 1602 (aromatic C=C), 1509, 1489, 1368, 1278, 1247 (aromatic ether linkage), 1160, 1013, and 961 (oxadiazole ring).

Their chemical structures are presented in Figure 1. All spectroscopy-grade solvents and all metal salts were purchased from various commercial sources and used without further purification as received.

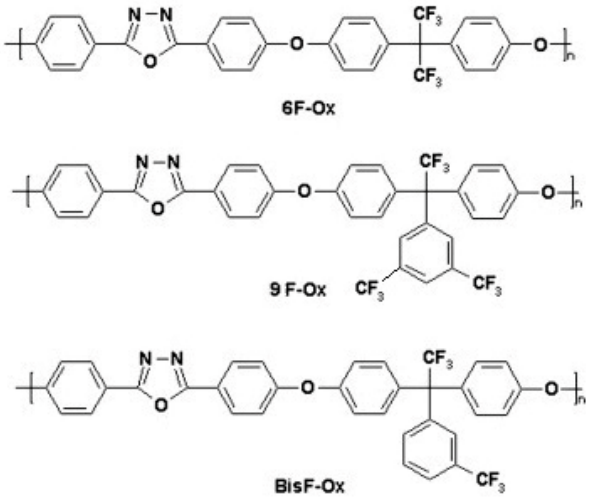

Figure 1. Structures of the poly(1,3,4-oxadiazole-ether) derivatives investigated in this study.

2.2. UV–Visible Absorption and Steady-State Fluorescence Spectra Measurements

The recognition of metal ions, including Mg^{2+}, Mn^{2+}, Ni^{2+}, Cd^{2+}, Zn^{2+}, Co^{2+}, Cu^{2+}, Hg^{2+}, Sn^{2+}, and Ag^{+} by **fluorinated 1,3,4-oxadiazole derivatives** in THF solution, was studied using absorption and fluorescence titration experiments. To prepare the metal ion stock solutions (1.05×10^{-3} mol L^{-1}), the proper amounts of $MgCl_2 \times 6H_2O$, $MnSO_4 \times H_2O$, $NiCl_2 \times 6H_2O$, $CdSO_4$, $ZnSO_4 \times 6H_2O$, $CoCl_2 \times 6H_2O$, $CuCl_2 \times 6H_2O$, $HgCl_2$, $SnCl_2 \times 2H_2O$, and $AgNO_3$ were dissolved in THF solvent, and these solutions were sonicated for 10 min to homogenize. In a fixed volume of fluorinated 1,3,4-oxadiazole assemblies (2.5 mL THF solution, 1×10^{-5} mol L^{-1}), a microliter syringe was used to gradually add different quantities of metal ion solutions (0–1500 µL), and then changes in the absorption and emission profiles were examined. Tetrahydrofuran (THF) was chosen as the solvent in this work, because it is an organic solvent in which fluorinated derivatives containing 1,3,4-oxadiazole units are soluble. Other probes used for the detection of Ag^{+}, Co^{2+}, and Cu^{2+} operating in solvents, such as THF, are presented in the literature [40,41].

For the absorption and fluorescence measurements, we employed an Analytic Jena 210+ spectrophotometer and photoluminescence spectrofluorometer LS55 (Perkin Elmer, Ltd., Waltham, MA, USA), respectively. A 20 kW xenon discharge lamp was used as the light source for the photoluminescence spectrofluorometer. Emission spectra were collected at an excitation wavelength corresponding to the maximum absorption value. All measurements were made at room temperature and recorded using a transparent quartz cuvette (with a 1 cm × 1 cm light path length). Furthermore, the experimental absorption and fluorescence spectral data of **BisFOx** reported in our previous work [39] were used to calculate the NLO parameters in different solvents.

2.3. Methods of the Evaluation of NLO Properties

For the determination of the first polarizability (α_{CT}), the hyperpolarizability (β_{CT}), and the second hyperpolarizability (γ_{CT}), the polarizability (α_{CT}) for the **BisFOx** derivative was calculated using the solvatochromic method, using Equation (1) [42,43]:

$$\alpha_{CT} = \alpha_{XX} = 2\frac{\mu_{eg}^2}{E_{eg}} = 2\frac{\mu_{eg}^2 \lambda_{eg}}{hc} = 2\frac{\mu_{eg}^2}{hc\,\nu} \quad (1)$$

where ν (cm^{-1}) and μ_{eg} are the wavenumber of the absorption maximum and transition dipole moment, respectively, which is defined by the oscillator strength f, Equation (2): x—the direction of charge transfer:

$$\mu_{eg}^2 = \frac{3e^2h}{8\pi^2mc} \times \frac{f}{\nu_{eg}} = 2.13 \times 10^{-30} \times \frac{f}{\nu_{eg}} \quad (2)$$

In Equation (2),

- m = mass of an electron (9.109×10^{-28} g);
- ν_{eg} = absorption frequency (in cm^{-1});
- h = Planck's constant (6.626×10^{-27} erg s);
- c = light velocity in vacuum (2.997×10^{10} cm s^{-1});
- e = charge on an electron (4.80×10^{-10} e.s.u.);
- f = oscillator strength for the charge transfer band (CT) determined using Equation (3).

$$f = \frac{2303\ m\ c^2}{\pi N_A e^2} \int \varepsilon(\nu) d\nu = 4.39 \times 10^{-9} \int \varepsilon(\nu) d\nu \quad (3)$$

In Equation (3), the constants "m", "e", and "c" are identical to those in Equation (2); N_A is the Avogadro's number ($6.32891937 \times 10^{23}$ m·kg^{-2}·s^{-1}), and $\int \varepsilon(\nu) d\nu$ is the area of the transition band considered, and is calculated using Equation (4):

$$\int \varepsilon(\nu) d\nu = 1.06 \times \varepsilon \times \Delta\nu_{1/2} \quad (4)$$

In Equation (4),

- ε = molar absorption coefficient (L mol^{-1}·cm^{-1});
- $\Delta\nu_{1/2}$ = full frequency width at half the maximum of the absorption band (cm^{-1}).

Hence, as understood according to Equations (2)–(4), μ_{eg} depends on the oscillator strength, f, which can be obtained from the solvatochromic information.

To estimate the values of the first hyperpolarizability (β_{CT}) parameter, we used a theory called "two-level microscopic models" [42], which was expressed by the following relationship (5):

$$\beta_{CT} = \frac{3\nu_{eg}^2 \mu_{eg}^2 \Delta\mu_{CT}}{2h^2c^2\left(\nu_{eg}^2 - \nu_L^2\right)\left(\nu_{eg}^2 - 4\nu_L^2\right)} \quad (5)$$

In Equation (5), ν_{eg} = frequency of the reference incident radiation at which the β_{CT} value would be mentioned:

- h and c = similar constants as in Equation (2);
- $\Delta\mu_{CT} = (\mu_e - \mu_g)^2$ = the transition dipole moment (the difference between the ground and excited states). Assuming $\nu_L = 0$ (no excitation), then Equation (5) transforms into:

$$\beta_{xxx} = \beta_{CT} = \frac{3\mu_{eg}^2 \Delta\mu_{CT}}{2(E_{max})^2} \quad (6)$$

In Equation (6), E_{max} = energy at the charge transfer absorption, which is calculated using the expression $E_{max} = hc/\lambda max = hc\nu$.

Second-order hyperpolarizability (γ_{CT}) was calculated with the solvatochromic data using a three-level model [43–46], with the following Equation (7):

$$\langle\gamma_{CT}\rangle = \frac{1}{E_{eg}^3} \mu_{eg}^2 \left(\Delta\mu^2 - \Delta\mu_{eg}^2\right) \quad (7)$$

Furthermore, to evaluate the dipole moment differences ($\Delta\mu = \mu_e - \mu_g$) of the **BisFOx** sample, we assumed that its environmental sensitivity is described by the Lippert–Mataga model (Equation (8)) [47]:

$$\nu_{max}^{abs} - \nu_{max}^{em} = mf_{LM}(\varepsilon, n) + cons\,tan\,t \quad (8)$$

$$f_{LM}(\varepsilon, n) = \frac{\varepsilon - 1}{\varepsilon + 2} - \frac{n^2 - 1}{n^2 + 2} \quad (9)$$

Thus, Equation (8) can be rewritten as the following:

$$\nu_{max}^{abs} - \nu_{max}^{em} = \frac{2\Delta f_{LM}}{hca^3}\left(\mu_e - \mu_g\right)^2 + cons\,tan\,t \quad (10)$$

In Equation (10), $\nu_{max}^{abs} - \nu_{max}^{em}$ = solvatochromic shift (cm^{-1}) is the difference between the fluorescence and absorption bands; ε = the relative permittivity (Table 1); n = the refractive indexes that were taken from [48] (Table 1); μ_g, μ_e = the dipole moments of the ground state and excited states; $\left(\mu_e - \mu_g\right)^2$ = the transition dipole moment, which is proportional to the slope of the Lippert–Mataga plot (Figure 2); h and c are the same as those defined in Equation (2), and "a" is the solvent cavity (Onsager) radius (its calculation is given in Supplementary Material (Equations (S1)–(S5) and Table S1)).

Table 1. Photophysical characteristics, Lippert-Mataga polarity function, and spectral data for **BisFOx** molecules, in different solvents.

Media [a]	ε [b]	n [c]	$f_{LM}(\varepsilon,n)$ [d]	ν_{max}^{abs}, cm^{-1} [e]	ν_{max}^{em}, cm^{-1} [f]	$\Delta\nu$, cm^{-1} [g]
DIO	2.25	1.4224	0.0245	33,333	28,169	5164
TOL	2.38	1.4961	0.0135	33,112	28,089	5022
CHCl3	4.81	1.4459	0.1483	33,003	27,855	5148
THF	7.47	1.4070	0.2084	33,333	28,169	5164
CH_3OH	33.00	1.3288	0.3086	35,088	27,778	5667
DMF	38.25	1.4305	0.2752	33,333	27,933	5400
DMSO	47.24	1.4770	0.2640	33,333	27,778	5555

[a] Solvents: dioxane (DIO), toluene (TOL), chloroform ($CHCl_3$), tetrahydrofuran (THF), methanol (CH_3OH), dimethylformamide (DMF), dimethyl sulfoxide (DMSO); [b] ε and [c] n—dielectric constants and refractive indexes that were taken from [48]; [d] the Lippert–Mataga polarity function ($f(\varepsilon) - f(n^2)$); [e] and [f] wavelength values for the absorption and emission maxima; [g] $\Delta\nu = \nu_{max}^{abs} - \nu_{max}^{em}$ is the solvatochromic shift (in cm^{-1}).

Using the slope of the linear part of the $\nu_{max}^{abs} - \nu_{max}^{em}$ vs. $f(\varepsilon) - f(n^2)$ plot (Figure 2), we have calculated the dipole moment differences for the **BisFOx** sample and found it to be 6.54 D.

2.4. Generalized Mulliken–Hush Method (GMH) for the Study of ICT Characteristics

The intramolecular charge transfer (ICT) features of the **BisFOx** sample were studied using a generalized GMH analysis based on the charge transfer band values from the absorption spectra, and using Equations (11)–(13) [49]:

$$C_b^2 = \frac{1}{2}\left(1 - \sqrt{\frac{\Delta\mu_{ge}^2}{\Delta\mu_{ge}^2 + 4\mu_{ge}^2}}\right) \quad (11)$$

$$H_{DA} = \frac{\mu_{ge}\Delta E_{ge}}{\Delta\mu_{ab}} = \frac{\mu_{ge}\Delta E_{ge}}{\sqrt{\Delta\mu_{ge}^2 + 4\mu_{ge}^2}} \quad (12)$$

$$R_{DA} = 2.06 \times 10^{-2}\frac{\sqrt{\Delta E_{ge}\varepsilon_{max}\Delta\nu_{1/2}}}{H_{DA}} \quad (13)$$

In Equations (11)–(13),

- C_b^2 = the electronic delocalization degree;
- H_{DA} = the electronic coupling matrix (strength of electronic coupling between the ground (S_0) and the charge transfer excited states (S_1));
- R_{DA} = the donor acceptor separation;
- ΔE_{ge} = the vertical excitation energy;
- $\Delta \mu_{ge}^2$ = the transition dipole moments;
- ε_{max} = the molar extinction coefficient at maximum absorption ($M^{-1} \cdot cm^{-1}$);
- $\Delta \nu_{1/2}$ = the width of the band at $A = A_{max}/2$ (cm^{-1}).

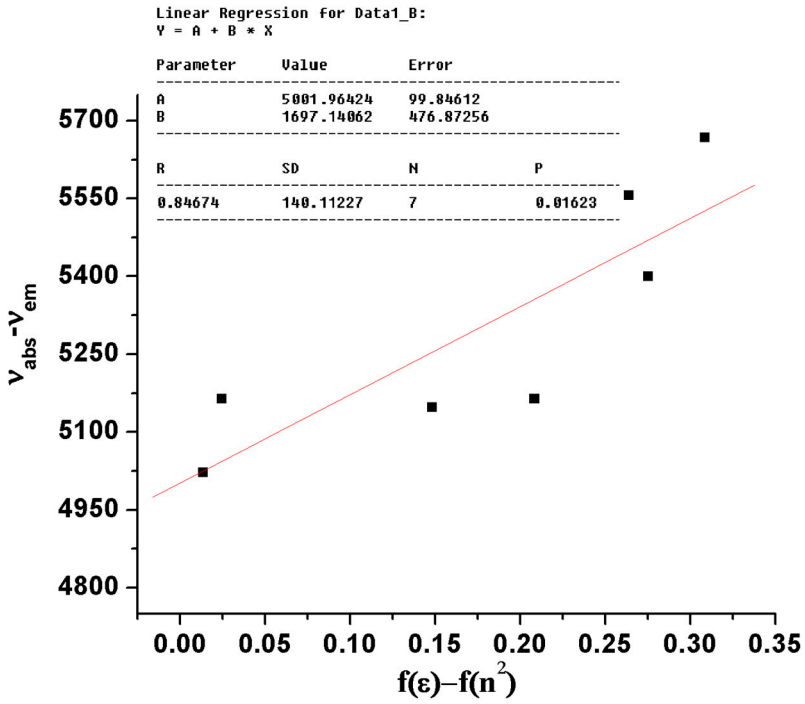

Figure 2. Plot and fit line of $\nu_{max}^{abs} - \nu_{max}^{em}$ against the Lippert–Mataga solvent polarity function ($f(\varepsilon) - f(n^2)$) for the **BisFOx** compound (in a series of solvents).

3. Results and Discussion

3.1. Recognition of Metal Ions by Fluorinated 1,3,4-Oxadiazole Derivatives

Interactions of the **BisFOx**, **9FOx**, and **6FOx** derivatives with various metal ions in tetrahydrofuran solutions were investigated on the basis of modifications in the optical spectra caused by increasing concentrations of these metal ions. Figure 3a shows the modifications in the absorption spectra of the **BisFOx** sample alone and when 1500 µL of each of the selected metal cations (M^{n+} = Mg^{2+}, Mn^{2+}, Ni^{2+}, Cd^{2+}, Zn^{2+}, Co^{2+}, Cu^{2+}, Hg^{2+}, Sn^{2+}, and Ag^{+}) has been added. Pure **BisFOx** sample in the THF solvent showed a strong absorption band located between 270 and 310 nm (having λ_{max}^{abs} at 302 nm) that was assigned to the π-π^* transitions of the 1,3,4-oxadiazole ring. From Figure 3a, it is obvious that after additions of the Ag^{+}, Co^{2+}, and Cu^{2+} ions, important variations were detected in the absorption spectra. Instead, there were no remarkable responses to the other metals tested. Similar behaviors were observed for the samples **9FOx** (Figure 3b) and **6FOx** (Figure 3c), with the mention that the absorption bands at 300 and 366 nm, in the case of sample **6FOx**, which appeared after the addition of 1500 µL Co^{2+}, was much better structured than those that appeared for the **BisOx** and **9FOx** samples.

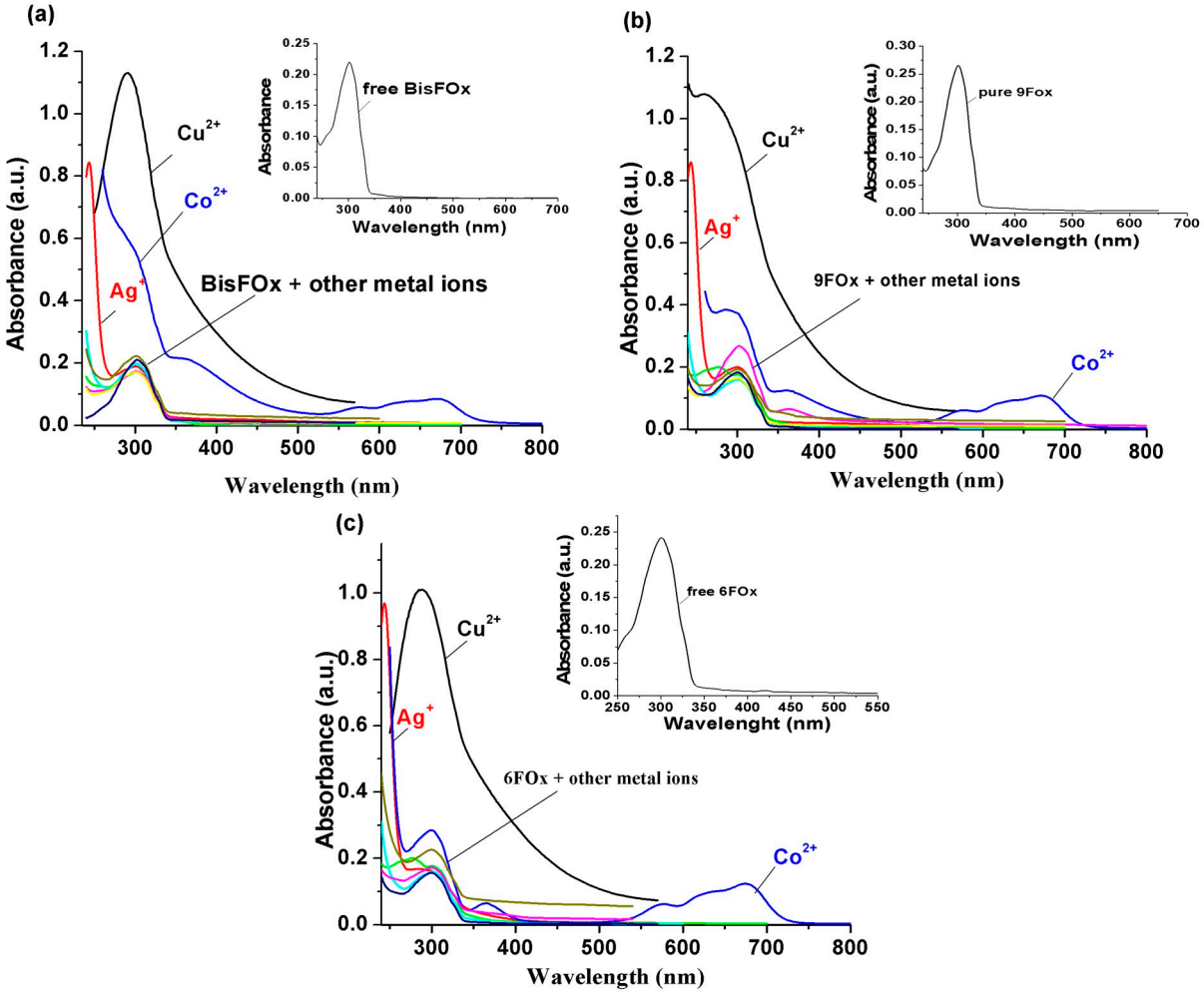

Figure 3. Absorption changes of (**a**) **BisFOx**, (**b**) **9FOx**, and (**c**) **6FOx** samples, when adding 1500 μL of various interfering ions (Mg^{2+}, Mn^{2+}, Ni^{2+}, Cd^{2+}, Zn^{2+}, Co^{2+}, Cu^{2+}, Hg^{2+}, Sn^{2+}, and Ag^{+}). The inset shows the absorption spectra of the free **BisFOx**, **9FOx**, and **6FOx**, in THF solution.

Absorption titration spectra of the sample **BisFOx** in THF solution (Figure 3a), upon the gradual addition of Ag^{+} ions, showed that the absorption band intensity (at 302 nm) was reduced linearly and a new absorption band appeared at 244 nm, whose intensity progressively increased with Ag^{+} concentration.

Additionally, notable modifications in the absorption spectral profile were observed when Co^{2+} ions (0–1500 μL) were added to the solution of the **BisFOx** sample; i.e., the intensity at λ_{max}^{abs} = 302 nm gradually increased, accompanied by the appearance of a new band (550–700 nm) with λ_{max} at 674 nm and a weak shoulder at 570 nm (Figure 4b), the intensity of which increased with an increasing concentration of Co^{2+} ions. Moreover, this new absorption band was probably due to **BisFOx**-to-metal charge-transfer (LMCT), rather than Co-based d–d transitions [50]. Instead, as shown in Figure 4b, the absorption band intensified (even for the whole spectrum) when the **BisFOx** sample was titrated with Co^{2+} ions (the opposite trend was observed after titration with Ag^{+}). This behavior could be the result of electronic changes as a result of the creation of coordination bonds and/or deprotonation. Table 2 summarizes the changes in the absorption and fluorescence spectra of the **BisFOx** and **9FOx** samples after titrations with 1500 μL of different metal ions (also shown in Figure 3).

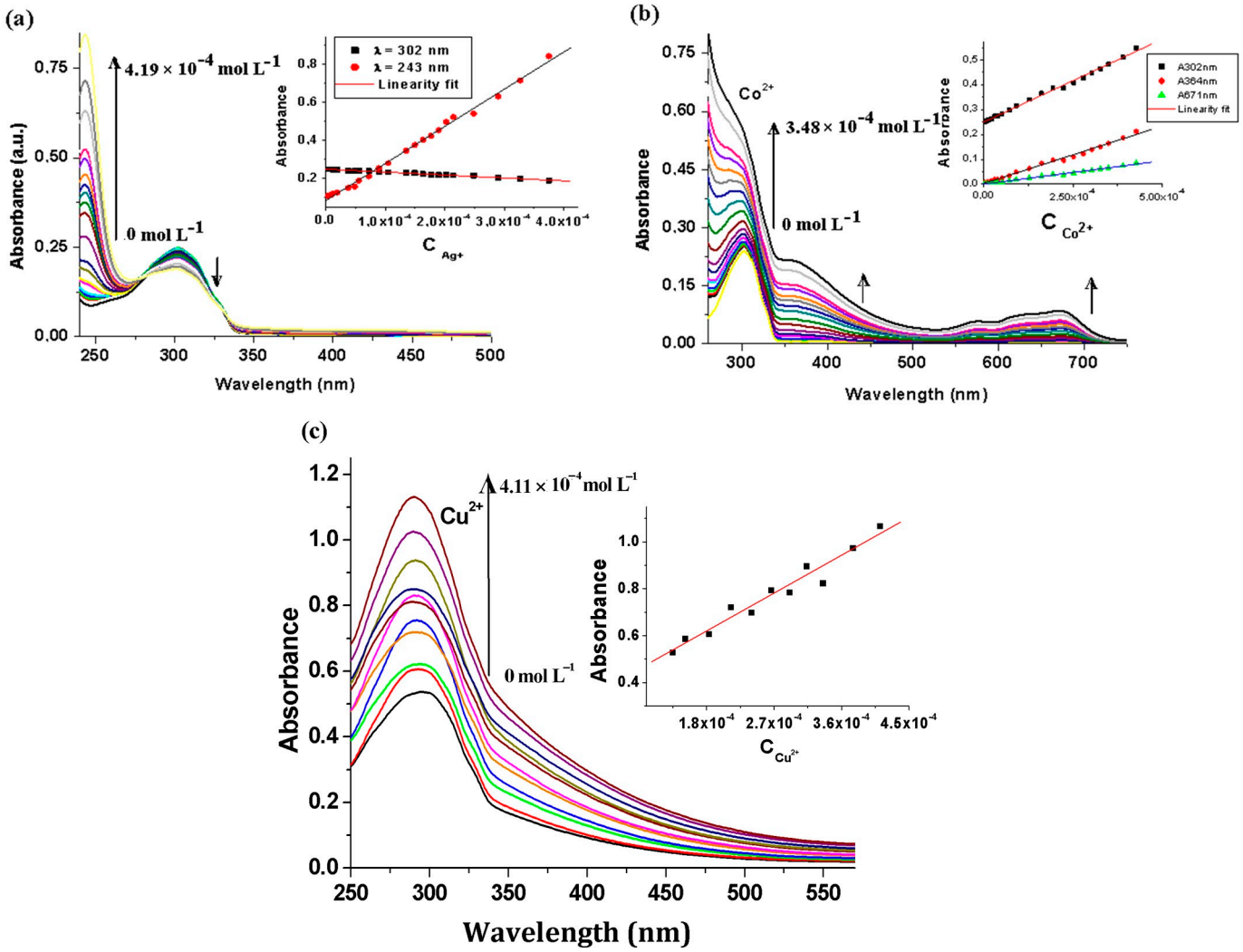

Figure 4. Plots depicting the effects of increasing amounts of (**a**) Ag^+, (**b**) Co^{2+}, and (**c**) Cu^{2+} metal ions on the absorption spectra for the **BisFOx** sample (c = 1 × 10^{-5} mol L^{-1}), in THF solution. Insets: The plot depicting the linear proportional relationship between the absorbance and the concentration of the Ag^+, Co^{2+}, and Cu^{2+} ions.

After the addition of copper ions, alongside the enhancement of absorption (λ_{max}^{abs} = 302 nm), a slight bathochromic shift of the band from 290 nm was detected (Figure 4c). A similar behavior of the **9FOx** derivative occurred when incremental quantities of Ag^+, Co^{2+}, and Cu^{2+} ions were added. From the plots of absorbance versus concentrations of Ag^+, Co^{2+}, and Cu^{2+} ions (insets in Figure 4a–c), we can observe a linear relation between the absorbance and the concentrations of these ions. For all spectral changes caused by Ag^+, Co^{2+}, and Cu^{2+} ions in the fluorinated 1,3,4-oxadiazole derivatives **BisFOx**, **9FOx**, and **6FOx** solutions, the linear regression equations and the corresponding data are listed in Table 3.

Quantitatively, the sensitivity of each **fluorinated 1,3,4-oxadiazole derivative** was evaluated using the values of the detection limits (LODs). The calculated values of LODs were obtained to be in the range 10^{-7}–10^{-8} M (Table 3). A better LOD, such as 8.533 × 10^{-6} M of Cu^{2+} ions, was obtained using the interactions of Cu^{2+} with the **9FOx** derivative. Moreover, these LOD values were compared with other different values for various molecular structures containing 1,3,4-oxadiazole from the literature, and these are shown in Table 3. We observe that the LOD values of the **BisFOx** were quite close in value to those of the 1,3,4-oxadiazole-containing compounds reported in Ref. [51] for detecting Cu^{2+}, as listed in Table 4. The absorption spectral patterns of **9FOx** and **6FOx** were almost similarly affected

by titration with Ag^+, Co^{2+}, and Cu^{2+} cations, except for the **6FOx** sample, upon titration with copper ions, when the absorption bands were better structured (Figures S1 and S2, from the Supplementary Material).

Table 2. Spectral data and optical responses of the **BisFOx** and 9FOx samples in the presence of different metal ions, in the THF solution.

Compounds	Absorption		Fluorescence	
	λ_{max}^{abs}, nm	A_0/A	λ_{max}^{em}, nm	F_0/F
BisFOx	302	-	356.5	-
BisFOx/Mg^{2+}	302	1.307	355	1.37
BisFOx/Mn^{2+}	302	1.279	356.5	1.24
BisFOx/Ni^{2+}	302	-	356.5	1.36
BisFOx/Cd^{2+}	302	1.297	356.5	1.32
BisFOx/Zn^{2+}	303	1.150	357	1.15
BisFOx/Co^{2+}	302 (sh)/570 (sh)/674	0.437	355.5	2.70
BisFOx/Cu^{2+}	291	0.495	357.5	2.98
BisFOx/Hg^{2+}	302	1.381	356	1.24
BisFOx/Sn^{2+}	301	1.156	356.5	1.28
BisFOx/Ag^+	244/301	0.189	356.5	2.03
9FOx	300	-	356	-
9FOx/Mg^{2+}	302/364 (weak)	0.9182	356	1.38
9FOx/Mn^{2+}	301	1.1756	356.5	1.21
9FOx/Ni^{2+}	265 (sh)/304 (sh)	1.3492	356	1.28
9FOx/Cd^{2+}	276/301 (sh)	0.7374	357.0	1.23
9FOx/Zn^{2+}	301	1.2989	357.0	1.16
9FOx/Co^{2+}	302/375 (sh)/570 (sh)/674	0.6346	-	-
9FOx/Cu^{2+}	273 (sh)	0.3364 [a]	356.5	2.90
9FOx/Hg^{2+}	301	1.4025	357	1.25
9FOx/Sn^{2+}	301	1.2176	356.5	1.24
9FOx/Ag^+	243 (sh)/300	1.3303	356	2.26

λ_{max}^{abs} and λ_{max}^{em}—the wavelength of the absorption and emission bands, respectively; A_0 and A—the intensity of the absorption band in the absence (A_0) and presence (A) of ~1500 µL solution of different metal ions; F_0 and F—emission intensities of the maximum of the emission band in the absence (F_0) and presence (F) of ~1500 µL of different metal ions, respectively; [a]—the values of F were read at a maximum of the emission band in the presence of 850 µL Ag^+ ions; sh—shoulder.

Table 3. Linear regression equation (LRE) and calculated parameters (LOD, LOQ) from plots between the absorption intensity and the concentrations of Ag^+, Co^{2+}, and Cu^{2+} ions, for **BisFOx**, **9FOx**, and the **6FOx** samples.

Parameters	BisFOx	9FOx	6FOx
		Ag^+	
LRE	$A = 0.083 - 1953.388C_{Ag+}$ (R^2 = 0.997, SD = 0.0148)	$A = 0.101 + 1989.96C_{Ag+}$ (R^2 = 0.999, SD = 0.0065)	$A = 0.156 + 2096.73C_{Ag+}$ (R^2 = 0.998, SD = 0.0137)
[a] LOD (µg L^{-1})	2.287×10^{-5}	9.784×10^{-6}	1.973×10^{-5}
[b] LOQ (µg L^{-1})	7.63×10^{-5}	3.261×10^{-5}	6.577×10^{-5}
		Co^{2+}	
LRE	$A = 0.249 + 667.87C_{Co2+}$ (R^2 = 0.997, SD = 0.0063)	$A = 0.210 + 369.20C_{Co2+}$ (R^2 = 0.999, SD = 0.0018)	$A = 0.0007 + 318.74C_{Co2+}$ (R^2 = 0.999, SD = 0.0016)
[a] LOD (µg L^{-1})	2.834×10^{-5}	1.463×10^{-5}	1.544×10^{-4}
[b] LOQ (µg L^{-1})	9.448×10^{-5}	4.875×10^{-5}	5.145×10^{-4}
		Cu^{2+}	
LRE	$A = 0.296 + 1794.53C_{Cu2+}$ (R^2 = 0.976, SD = 0.0379)	$A = 0.184 + 2179.85C_{Cu2+}$ (R^2 = 0.999, SD = 0.0062)	$A = 0.237 + 1994.80C_{Cu2+}$ (R^2 = 0.994, SD = 0.02373)
[a] LOD (µg L^{-1})	6.341×10^{-5}	8.533×10^{-6}	3.569×10^{-5}
[b] LOQ (µg L^{-1})	2.114×10^{-4}	2.844×10^{-5}	1.19×10^{-4}

[a] LOD—is the detection limit, estimated on the basis of the 3 Sb/m relation; [b] LOQ—is the limit of quantification, estimated on the basis of 10 Sb/m [50] (Sb = the standard deviation of the blank; m = the slope of calibration curve, respectively).

Table 4. Comparison of the LOD values of the prepared **BisFOx**, **9FOx**, and **6FOx** with some recently published chemosensors containing 1,2,4-oxadiazole rings [29,51–53] used for the determination of Ag+, Co^{2+}, and Cu^{2+} ions.

Materials	Metal Ions	LODs	Refs.
2,5-diphenyl-1,3,4-oxadiazole	Cu^{2+}	4.8×10^{-7} M	[51]
pyrazole-containing oxadiazole derivative	Cu^{2+}	2.14 μM	[29]
asymmetrical oxadiazole derivative	Co^{2+}	3.92×10^{-6} mol/L	[52]
polytriazoles derivative	Ag^{+}	4.22×10^{-7} M	[53]
BisFOx	Cu^{2+}	1.013×10^{-7} M	This study
BisFOx	Co^{2+}	4.52×10^{-8} M	This study
BisFOx	Ag^{+}	4.52×10^{-8} M	This study
9FOx	Cu^{2+}	1.45×10^{-8} M	This study
9FOx	Co^{2+}	1.45×10^{-8} M	This study
9FOx	Ag^{+}	1.66×10^{-8} M	This study
6FOx	Cu^{2+}	6.426×10^{-8} M	This study
6FOx	Co^{2+}	2.78×10^{-7} M	This study
6FOx	Ag^{+}	3.55×10^{-8} M	This study

Furthermore, the sensing abilities of the **BisFOx** and **9FOx** derivatives for Mg^{2+}, Mn^{2+}, Ni^{2+}, Cd^{2+}, Zn^{2+}, Co^{2+}, Cu^{2+}, Hg^{2+}, Sn^{2+}, and Ag^{+} ions, in THF solution were evaluated using their fluorescence spectra. The intensity of the emission bands (at 356 and 370 nm) were moderately quenched (FIQ—fluorescence intensity quenching) along with an increasing concentration of Ni^{2+}, Cd^{2+}, Hg^{2+}, Mn^{2+}, Sn^{2+}, and Zn^{2+}, but remarkable changes were recorded after gradually adding Ag^{+}, Co^{2+}, and Cu^{2+} ions (see the values for F_0/F, from Table 2 and Figure 5). The spectral variations observed in the fluorescence spectra of the **BisFOx** sample, upon the addition of incremental amounts of Ag^{+}, Co^{2+}, and Cu^{2+} cations, are illustrated in Figure 5a–c. Similarly, the fluorescence intensities at 356 and 370 nm were reduced to the same extent for the **9FOx** and **6FOx** systems, in the presence of incremental amounts of Ag^{+}, Co^{2+}, and Cu^{2+} ions, as for the sample **BisFOx** (see Figures S3 and S4, from the Supplementary Material).

The quenching extent (efficacy) of the systems under study was calculated using the following relation ($QE\% = (F_0 - F)/F_0 \times 100\%$) when 1500 μL of metal ions were introduced into the investigated solutions and various values were found for the different metal ions (Table 5). The fluorescence intensity was quenched to close to half of its initial value in the presence of Ag^{+}, Co^{2+}, and Cu^{2+} ions. The effect of cobalt ions was smaller (especially for the **6FOx** sample (35%)) than that of the copper and silver ions (Table 5). The **6FOx** derivative displayed a strong fluorescence reduction upon the addition of Ag^{+} ions (72%). The observed differences in the quenching effects of the metal ions may be due to the different values of electronegativity and the ionic radii of these metal ions [54,55].

Table 5. The efficiency of fluorescence quenching (%).

Codes	Ag^{+}	Co^{2+}	Cu^{2+}
BisFOx	50.92	54.33	66.62
9FOx	55.88	54.11	65.67
6FOx	72.73	35.83	65.24

Moreover, the variations in the values of A_0/A and F_0/F, calculated at ~302 and 356 nm for the **BisFOx** and **9FOx** samples, upon adding 1500 μL of the selected ions, have been listed in Table 2. The fluorescence quenching extent of the **BisFOx** and **9FOx** derivatives is variable for these metal ions (Tables 2 and 5, Figure 6). **9FOx** responds slightly better toward selected metal ions compared to the **BisFOx** sample. For example, the emission intensities are more highly quenched by Co^{2+} and Cu^{2+} ions, while the quenching extent by Ag^{+} is slightly lower (Table 5 and Figure 6). Additionally, the fluorescence responses of the samples **BisFOx** and **9FOx** to different metal ions are depicted at the two wavelengths

(356 and 370 nm) in the bar diagrams (Figure 6). Herein, it was found that for the Co^{2+} and Cu^{2+} ions only, the array of the two wavelengths could generate a distinct pattern response; namely, the F_0/F values were higher at 356 nm than at 370 nm, except for compound **9FOx** in the presence of copper ions. The maximum FIQ value is found in the presence of the Cu^{2+} ions.

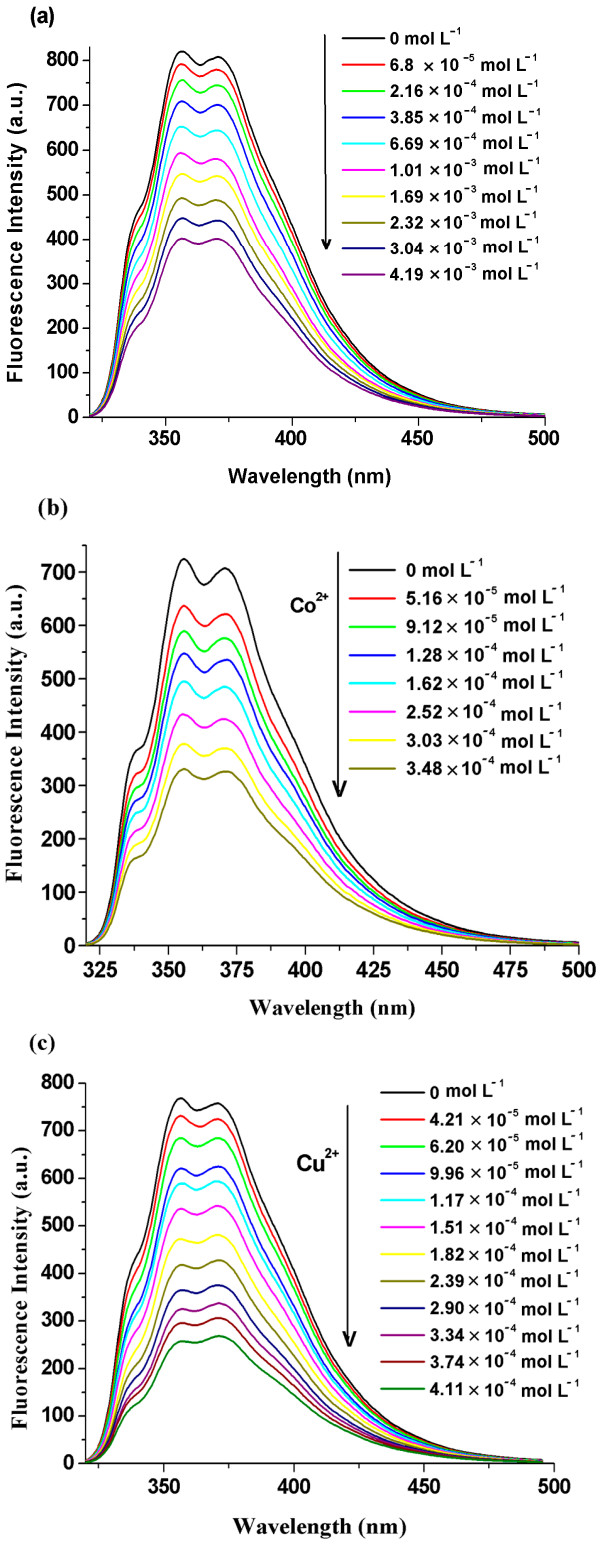

Figure 5. Emission spectra of the **BisFOx** compound (c = 1 × 10^{-5} mol L^{-1}), in THF solution, after titration with incremental amounts of Ag^+ (**a**), Co^{2+} (**b**), and Cu^{2+} (**c**) cations.

Moreover, in dimethyl sulfoxide (DMSO) solvent, which is considered to be a green solvent, we tested the sensing ability of the **BisFOx** sample to detect Cu^{2+} ions, and a similar form of behavior to that in THF was observed (Figure 7).

3.2. Nonlinear Optical Properties (NLO) Using the Solvatochromic-Based Approach

NLO properties of the fluorinated **BisFOx** derivative were investigated via the solvatochromic-based approach. In our previous studies [39,56], we reported the absorption and emission spectral data of the **BisFOx** derivative in solvents with various polarities. These data have been used in this paper to evaluate solvatochromic-dependent properties, including μ_{CT}, μ_{eg}^2, and oscillator strength (f), which are required to determine the NLO parameters (α_{CT}, β_{CT}, and γ_{CT}).

Detailed equations [57,58] used for calculations of $\Delta\mu_{CT}$ and a (the Onsager interaction radius of solute molecules) are given in the Materials (Section 2.1) and Methods and Supplementary Materials Sections. The obtained values for these spectroscopic physical parameters are listed in Table 6 and have been further used for the calculation of the α, β, and γ parameters (presented below).

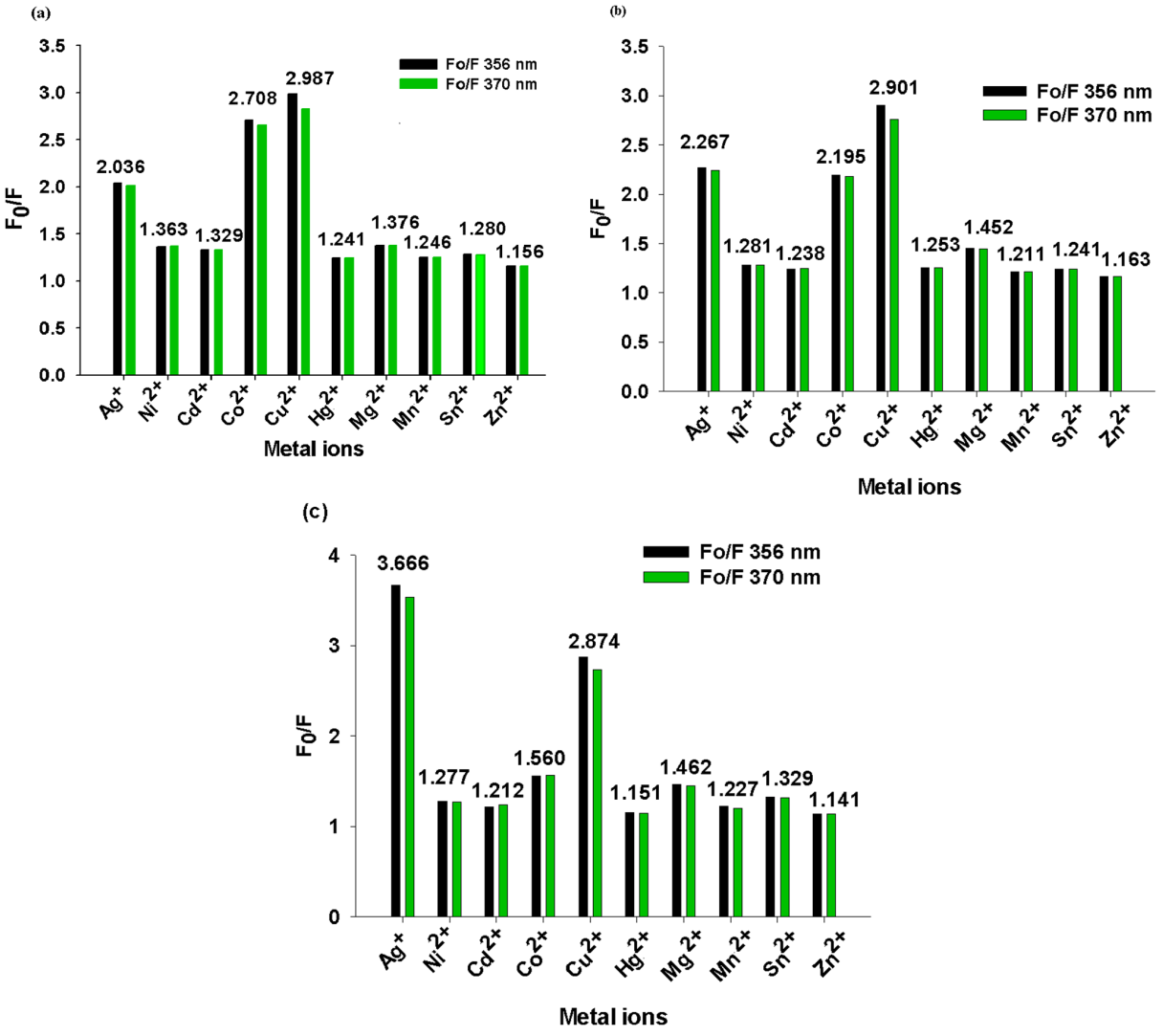

Figure 6. The degree of change in the emission intensity at two wavelengths (356 and 370 nm) after metal ion titration of the **BisFOx** (**a**) **9FOx** (**b**) and **6FOx** (**c**) samples in THF solution. Numerical values are for F_0/F corresponding to λem = 356 nm.

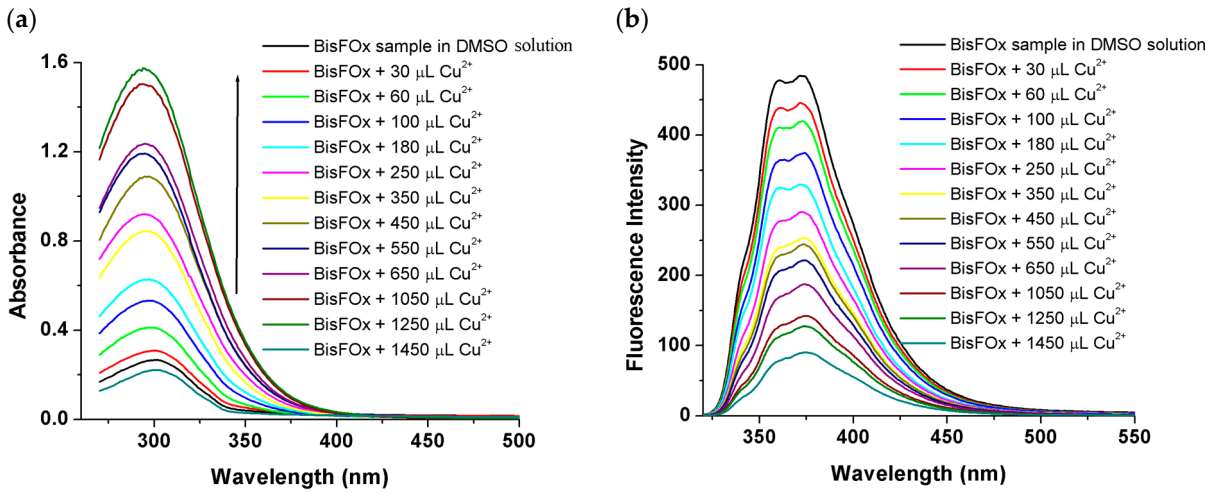

Figure 7. Absorption (**a**) and emission spectra (**b**) of the **BisFOx** compound (c = 1×10^{-5} mol L^{-1}), in DMSO solution, after titration with incremental amounts of Cu^{2+} ions.

Table 6. Calculated NLO and ICT parameters of the **BisFOx** sample in various solvents.

Media	f [a] e.s.u.	μ_{eg} [b] 10^{-35} e.s.u.	$\Delta\mu_{CT}$ [c] 10^{-17} e.s.u.	α_{CT} [d] 10^{-23} e.s.u.	β_{CT} [e] 10^{-32} e.s.u.	γ_{CT} [f] 10^{-34} e.s.u.	C_b^2 [g]	H_{DA} [h] cm^{-1}	R_{DA} [i] Å
DIO	0.6671	4.26	6.54	0.128	9.525	0.56	0.196	13,220	3.50
TOL	0.4339	2.79	6.54	0.084	6.320	0.39	0.120	10,745	3.46
$CHCl_3$	0.5527	3.56	6.54	0.108	8.130	0.49	0.162	12,152	3.45
THF	0.6173	3.94	6.54	0.119	8.814	0.53	0.180	12,824	3.47
CH_3OH	0.0495	0.30	6.54	0.086	6.05	0.03	0.001	1602	8.08
DMF	0.5929	3.78	6.54	0.114	8.465	0.50	0.173	12,615	3.46
DMSO	0.6983	4.46	6.54	0.134	0.010	0.58	0.204	13,440	3.52

[a–i]—parameters defined by Equations (1)–(13). **Solvent abbreviations:** DIO (dioxane, ε = 2.25); TOL (toluene, ε = 2.38); $CHCl_3$ (chloroform, ε = 4.81); THF (tetrahydrofuran, ε = 7.47); CH_3OH (methanol, ε = 33.00); DMF (*N*,*N*-dimethylformamide, ε = 38.25); DMSO (dimethyl sulfoxide, ε = 47.24).

The calculated values for the NLO parameters (α_{CT}, β_{CT}, and γ_{CT}) of the **BisFOx** compound are shown in Table 6. The highest values were found for the α_{CT} and β_{CT} parameters (0.128×10^{-23} and 9.525×10^{-32} e.s.u., respectively) in dioxane (DIO) media. Additionally, a rather high value was obtained for the β_{CT} parameter in DMF (8.46×10^{-32} e.s.u.) solution. Instead, the lowest β_{CT} for **BisFOx** is found in the DMSO solution, which may be due to the influence of its viscosity (resistance to the twisting of molecules) and polarity on its electronic structure and its NLO properties [59]. Moreover, for the γ_{CT}-NLO parameter of the analyzed fluorinated derivative, the highest value of 0.58×10^{-34} e.s.u. was observed in the DMSO solution, while the lowest value of 0.03×10^{-34} e.s.u. was obtained in the CH_3OH medium. Changes in NLO parameters as a function of solvent may be due to the properties of the microenvironment (the viscosity and polarity of DMSO) affecting the structural changes of the **BisFOx** molecules.

Table 6 lists the obtained values of the ICT-intramolecular charge transfer characteristics for **BisFOx** in selected solvents. Generally, when the C_b^2 values are close to zero, this indicates a total delocalization of charges, and when C_b^2 equals 1, this suggests a total localization of the charge in the system [60]. The electronic delocalization degree of the **BisFOx** derivative in all of the selected media tends strongly towards zero, indicating a maximum delocalization of the charge of this fluorinated 1,3,4-oxadiazole derivative. The electronic coupling matrix (H_{DA}) defines the charge transfer rate of the D-π-A structures and differs contrariwise with the R_{DA} values. For the **BisFOx** sample, the lowest values of the electronic coupling matrix were found in methanol, while the highest values were

found in the DMSO medium (Table 6). Instead, the lowest values of the separation acceptor donor parameter were found in methanol.

4. Conclusions

In summary, the ability of some **fluorinated 1,3,4-oxadiazole derivatives** to recognize metal ions was investigated by monitoring changes in the absorption and fluorescence spectral patterns of these compounds. Our derivatives were found to be particularly sensitive to silver, cobalt, and copper ions. Finally, the NLO responses and intermolecular charge transfer (ICT) characteristics for the **BisFOx** derivative were evaluated via the solvatochromic method. The investigated fluorinated 1,3,4-oxadiazole derivatives exhibited good NLO parameters and ICT characteristics in selected solvents, and it was observed that the environment affects the properties of the studied compounds.

Supplementary Materials: The following supporting information can be downloaded at: https://www.mdpi.com/article/10.3390/chemosensors10050183/s1, 1H NMR data. Figure S1: Absorption spectral changes during the titration of the 9FOx sample (c = 1 × 10^{-5} mol L^{-1}) with incremental amounts of Ag^{+} (a), Co^{2+} (b), and Cu^{2+} (c) cations; Figure S2: Absorption spectral changes during the titration of the 6FOx sample (c = 1 × 10^{-5} mol L^{-1}) with incremental amounts of Ag^{+} (a), Co^{2+} (b), and Cu^{2+} (c) cations; Figure S3: Fluorescence spectral changes during the titration of the 9FOx sample (c = 1 × 10^{-5} mol L^{-1}) with incremental amounts of Ag^{+} (a), Co^{2+} (b), and Cu^{2+} (c) cations; Figure S4: Fluorescence spectral changes during the titration of the 6FOx sample (c = 1 × 10^{-5} mol L^{-1}) with incremental amounts of Ag^{+} (a), Co^{2+} (b), and Cu^{2+} (c) cations; Table S1: Values of the atomic simple connectivity indices, δ and valence connectivity indices δ^{v} used for calculating zero- and first-order connectivity indices; Equations (S1)–(S5): used in calculating the Onsager cavity radius (a) for the BisFOx derivative.

Author Contributions: Conceptualization, M.H.; methodology, M.H. and A.A.; validation, C.H.; formal analysis, A.A.; investigation, A.M.I.; writing, M.H., A.M.I. and C.H. All authors have read and agreed to the published version of the manuscript.

Funding: This research received no external funding.

Institutional Review Board Statement: Not applicable.

Informed Consent Statement: Not applicable.

Data Availability Statement: Not applicable.

Acknowledgments: This work was supported by a grant of the Ministry of Research, Innovation and Digitization, CNCS/CCCDI-UEFISCDI, Romania, and project number PN-III-P1-1.1-TE-2019-0594, within PNCDI III.

Conflicts of Interest: The authors declare no conflict of interest.

References

1. Salassa, G.; Terenzi, A. Metal complexes of oxadiazole ligands: An overview. *Int. J. Mol. Sci.* **2019**, *20*, 3483. [CrossRef]
2. Puchkova, L.V.; Broggini, M.; Polishchuk, E.V.; Ilyechova, E.Y.; Polishchuk, R.S. Silver ions as a tool for understanding different aspects of copper metabolism. *Nutrients* **2019**, *1*, 1364. [CrossRef]
3. Pandey, N.; Mehata, M.S.; Fatima, N.; Pant, S. Modulation of fluorescence properties of 5-aminoquinoline by Ag^{+} in aqueous media via charge transfer. *J. Photochem. Photobiol. A* **2020**, *396*, 112549. [CrossRef]
4. Selvan, G.T.; Varadaraju, C.; Selvan, R.T.; Enoch, I.V.M.V.; Selvakumar, P.M. On/off fluorescent chemosensor for selective detection of divalent iron and copper ions molecular logic operation and protein binding. *ACS Omega* **2018**, *3*, 7985–7992. [CrossRef]
5. Siczek, K.; Zatorski, H.; Fichna, J. Silver and other metals in the treatment of gastrointestinal diseases. *Curr. Med. Chem.* **2015**, *22*, 3695–3706. [CrossRef]
6. Ojha, R.; Prasad, A.N. Menkes disease what a multidisciplinary approach can do. *J. Multidiscip. Healthc.* **2016**, *9*, 371–385. [CrossRef]
7. Członkowska, A.; Litwin, T.; Dusek, P.; Ferenci, P.; Lutsenko, S.; Medici, V.; Rybakowski, J.K.; Weiss, K.H.; Schilsky, M.L. Wilson disease. *Nat. Rev. Dis. Primers* **2018**, *4*, 21. [CrossRef]
8. Lan, A.P.; Chen, J.; Chai, Z.F.; Hu, Y. The neurotoxicity of iron, copper and cobalt in Parkinson's disease through ROS-mediated mechanisms. *BioMetals* **2016**, *29*, 665–678. [CrossRef]

9. Gorantla, N.V.; Landge, V.G.; Nagaraju, P.G.; Priyadarshini, P.; Balaraman, C.G.E.; Chinnathambi, S. Molecular cobalt (II) complexes for tau polymerization in alzheimer's disease. *ACS Omega* **2019**, *41*, 6702–6714. [CrossRef]
10. Kamnev, A.A.; Antonyuk, L.P.; Smirnova, V.E.; Serebrennikova, O.B.; Kulikov, L.A.; Perfiliev, Y. Trace cobalt speciation in bacteria and at enzymic active sites using emission Mössbauer spectroscopy. *Anal. Bioanal. Chem.* **2022**, *372*, 431–435. [CrossRef]
11. Zhao, R.-X.; Liu, A.-Y.; Wen, Q.-L.; Wu, B.-C.; Wang, J.; Hu, Y.-L.; Pu, Z.F.; Ling, J.; Cao, Q. Glutathione stabilized green-emission gold nanoclusters for selective detection of cobalt ion. *Spectrochim. Acta Part A Mol. Biomol.* **2021**, *254*, 119628. [CrossRef]
12. Wu, H.; Kong, D.; Ruan, Z.; Hsu, P.; Wang, S.; Yu, Z.; Carney, T.J.; Hu, L.; Fan, S.; Cui, Y. A transparent electrode based on a metal nanotrough network. *Nat. Nanotechnol.* **2013**, *8*, 421–425. [CrossRef]
13. Chernousova, S.; Epple, M. Silver as antibacterial agent: Ion, nanoparticle, and metal. *Angew. Chem. Int. Ed. Engl.* **2013**, *52*, 1636–1653. [CrossRef]
14. Yang, F.-Y.; Jiang, S.-J.; Sahayam, A.C. Combined use of HPLC-ICP-MS and microwave-assisted extraction for the determination of cobalt compounds in nutritive supplements. *Food Chem.* **2014**, *147*, 215–219. [CrossRef]
15. Diniz, K.M.; Gorla, F.A.; Ribeiro, E.S.; do Nascimento, M.B.O.; Correa, R.J.; Teixeira Tarley, C.R.; Segatelli, M.G. Preparation of $SiO_2/Nb_2O_5/ZnO$ mixed oxide by sol-gel method and its application for adsorption studies and on-line preconcentration of cobalt ions from aqueous medium. *Chem. Eng. J.* **2014**, *239*, 233–241. [CrossRef]
16. Mimendia, A.; Legin, A.; Merkoçi, A.; del Valle, M. Use of sequential injection analysis to construct a potentiometric electronic tongue: Application to the multideterminationof heavy metals. *Sens. Actuators B* **2010**, *146*, 420–426. [CrossRef]
17. Liu, S.; Wang, Y.-M.; Han, J. Fluorescent chemosensors for copper(II) ion: Structure, mechanism and application. *J. Photochem. Photobiol. C Photochem. Rev.* **2017**, *32*, 78–103. [CrossRef]
18. Awad, F.S.; AbouZied, K.M.; Bakry, A.M.; Abou El-Maaty, W.M.; El-Wakil, A.M.; El-Shall, M.S. Highly fluorescent hematoporphyrin modified graphene oxide for selective detection of copper ions in aqueous solutions. *Anal. Chim. Acta* **2020**, *1140*, 111–121. [CrossRef]
19. Bagheri, N.; Mazzaracchio, V.; Cinti, S.; Colozza, N.; Di Natale, C.; Netti, P.A.; Saraji, M.; Roggero, S.; Moscone, D.; Arduini, F. Electroanalytical sensor based on gold-nanoparticle-decorated paper for sensitive detection of copper ions in sweat and serum. *Anal. Chem.* **2021**, *93*, 5225–5233. [CrossRef]
20. Shellaiah, M.; Wu, Y.-H.; Singh, A.; Raju, M.V.R.; Lin, H.-C. Novel pyrene- and anthracene-based Schiff base derivatives as Cu^{2+} and Fe^{3+} fluorescence turn-on sensors and for aggregation induced emissions. *J. Mater. Chem. A* **2013**, *113*, 10–18. [CrossRef]
21. Lium, Q.; Bianm, W.; Shim, H.; Fanm, L.; Shuangm, S.; Dongm, C.; Choi, M.M.F. A novel ratiometric emission probe for Ca^{2+} in living cells. *Org. Biomol. Chem.* **2013**, *11*, 503–508. [CrossRef]
22. Liu, Q.; Feng, L.; Yuan, C.; Zhang, L.; Shuang, S.; Dong, C.; Hu, Q.; Choi, M.M.F. A highly selective fluorescent probe for cadmium ions in aqueous solution and living cells. *Chem. Commun.* **2014**, *502*, 498–501. [CrossRef]
23. Homocianu, M.; Ipate, A.M.; Homocianu, D.; Airinei, A.; Hamciuc, C. Metal ions sensing properties of some phenylquinoxaline derivatives. *Spectrochim. Acta A Mol. Biomol. Spectrosc.* **2019**, *215*, 371–380. [CrossRef]
24. Ambrosi, G.; Borgogelli, E.; Formica, M.; Fusi, V.; Giorgi, L.; Micheloni, M.; Rampazzo, E.; Sgarzi, M.; Zaccheroni, N.; Prodi, L. PluS Nanoparticles as a tool to control the metal complex stoichiometry of a new thio-aza macrocyclic chemosensor for Ag I, and Hg II, in water. *Sens. Actuators B Chem.* **2015**, *207*, 1035–1044. [CrossRef]
25. Zhang, Y.; Wang, G.; Zhang, J. Study on a highly selective fluorescent chemosensor for Fe^{3+} based on 1,3,4-oxadiazole and phosphonic acid. *Sens. Actuators B Chem.* **2014**, *200*, 259–268. [CrossRef]
26. Tang, L.; Zheng, Z.; Huang, Z.; Zhong, K.; Bian, Y.; Nandhakumar, R. Multi-analyte, ratiometric and relay recognition of a 2,5-diphenyl-1,3,4-oxadiazole-based fluorescent sensor through modulating ESIPT. *RSC Adv.* **2015**, *510*, 505–511. [CrossRef]
27. Lin, L.; Wang, D.; Chen, S.-H.; Wang, D.-J.; Yin, G.-D. A highly sensitive fluorescent chemosensor for selective detection of zinc II, ion based on the oxadiazole derivative. *Spectrochim. Acta A Mol. Biomol. Spectrosc.* **2017**, *174*, 272–278. [CrossRef]
28. Zhu, L.; Gu, C.; He, Y.; Wang, G. Study on a highly selective fluorescent chemosensor for Cu^{2+} and its direct sensing for proton based on 1,3,4-oxadiazole. *J. Lumin.* **2014**, *153*, 439–445. [CrossRef]
29. Liu, Y.; Fei, Q.; Shan, H.; Cui, M.; Liu, Q.; Feng, G.; Huan, Y. A novel fluorescent "off-on-off" probe for relay recognition of Zn^{2+} and Cu^{2+} derived from *N*,*N*-bis(2-pyridylmethyl)amine. *Analyst* **2014**, *139*, 1868. [CrossRef]
30. Zheng, C.; Yuan, A.; Zhang, Z.; Shen, H.; Bai, S.; Wang, H. Synthesis of pyridine-based 1,3,4-oxadiazole derivative as fluorescence turn-on sensor for high selectivity of Ag^{+}. *J. Fluoresc.* **2013**, *23*, 785–791. [CrossRef]
31. Al-Omary, F.A.M.; Mary, Y.S.; Panicker, C.Y.; El-Emam, A.A.; Al-Swaidan, I.A.; Al-Saadi, A.A.; Van Alsenoye, C. Spectroscopic investigations, NBO, HOMO–LUMO, NLO analysis and molecular docking of 5- adamantan-1-yl;-3-anilinomethyl-2,3-dihydro-1,3,4-oxadiazole-2-thione, a potential bioactive agent. *J. Mol. Struct.* **2015**, *1096*, 1–14. [CrossRef]
32. Li, Q.; Cui, L.-S.; Zhong, C.; Yuan, X.-D.; Dong, S.-C.; Jiang, Z.-Q.; Liao, L.S. Synthesis of new bipolar host materials based on 1,2,4-oxadiazole for blue phosphorescent OLEDs. *Dye. Pigment.* **2014**, *101*, 142–149. [CrossRef]
33. Lin, Y.; Li, Y.; Zhan, X. Small molecule semiconductors for high-efficiency organic photovoltaics. *Chem. Soc. Rev.* **2012**, *41*, 4245–4272. [CrossRef]
34. Choi, M.-H.; Kim, H.Y.; Lee, E.J.; Moon, D.K. Control of molecular curvature and crystallinity of quinacridone-benzoxadiazole copolymers using different pi bridge for polymer solar cells. *Polymer* **2016**, *91*, 162–173. [CrossRef]
35. Cristiano, R.; de Oliveira Santos, D.M.P.; Gallardo, H. Synthesis and characterization of low molecular mass luminescent liquid crystalline materials with 1,3,4-oxadiazole units. *Liq. Cryst.* **2005**, *32*, 7–14. [CrossRef]

36. Homocianu, M.; Airinei, A. 1,3,4-Oxadiazole derivatives; Optical properties in pure and mixed solvents. *J. Fluoresc.* **2016**, *26*, 1617–1635. [CrossRef]
37. Maidur, S.R.; Patil, P.S.; Rao, S.V.; Shkir, M.; Dharmaprakashd, S.M. Experimental and computational studies on second- and third-order nonlinear optical properties of a novel D-π-A type chalcone derivative 3-4-methoxyphenyl;-1- 4-nitrophenyl, prop-2-en-1-one. *Opt. Laser Technol.* **2017**, *97*, 219–228. [CrossRef]
38. Anitha, P.; Pathrose, B.P.; Radhakrishnan, P.; Mujeeb, A. Nonlinear optical properties of neutral red dye: Enhancement using laser ablated gold nanoparticles. *Opt. Laser Technol.* **2020**, *130*, 106338. [CrossRef]
39. Ipate, A.M.; Homocianu, M.; Hamciuc, C.; Airinei, A.; Bruma, M. Photophysical behavior of some aromatic poly1,3,4-oxadiazole-ethers derivatives. *Spectrochim. Acta A Mol. Biomol. Spectrosc.* **2014**, *123*, 167–175. [CrossRef]
40. Chandrasekaran, Y.; Dutta, G.K.; Kanth, R.B.; Patil, S. Tetrahydroquinoxaline based squaraines: Synthesis and photophysical properties. *Dye. Pigment.* **2009**, *83*, 162–167. [CrossRef]
41. Saleem, M.; Khang, C.H.; Kim, M.H.; Lee, K.H. Chromo/Fluorogenic detection of Co^{2+}, Hg^{2+} and Cu^{2+} by the simple Schiff base sensor. *J. Fluoresc.* **2016**, *26*, 11–22. [CrossRef]
42. Paley, M.S.; Harris, J.M.; Looser, H.; Baumert, J.C.; Bjorklund, G.C.; Jundt, D.; Twieg, R.J. A solvatochromic method for determining second-order polarizabilities of organic molecules. *J. Org. Chem.* **1989**, *543*, 774–3778. [CrossRef]
43. Abbotto, A.; Beverina, L.; Bradamante, S.; Facchetti, A.; Klein, C.; Pagani, G.A.; Redi-Abshiro, M.; Wortmann, R. A distinctive example of the cooperative interplay of structure and environment in tuning of intramolecular charge transfer in second-order nonlinear optical chromophores. *Chem. A Eur. J.* **2003**, *91*, 991–2007. [CrossRef]
44. Oudar, J.L.; Chemla, D.S. Hyperpolarizabilities of the nitroanilines and their relations to the excited state dipole moment. *J. Chem. Phys.* **1977**, *66*, 2664. [CrossRef]
45. Mahajan, P.G.; Dige, N.C.; Desai, N.K.; Patil, S.R.; Kondalkar, V.V.; Hong, S.K.; Lee, K.H. Selective detection of Co^{2+} by fluorescent nano probe Diagnostic approach for analysis of environmental samples and biological activities. *Spectrochim. Acta A Mol. Biomol. Spectrosc.* **2018**, *198*, 136–144. [CrossRef]
46. Şenkuytu, E.; Eçik, E.T. New hexa-bodipy functionalized dendrimeric cyclotriphosphazene conjugates as highly selective and sensitive fluorescent chemosensor for Co^{2+} ions. *Spectrochim. Acta A Mol. Biomol. Spectrosc.* **2018**, *198*, 232–238. [CrossRef]
47. Lippert, E.; Luder, W.; Boos, H. *Advances in Molecular Spectroscopy*; Pergamon: Oxford, UK, 1962.
48. Reichardt, C. *Solvents and Solvent Effects in Organic Chemistry*, 3rd ed.; Wiley-VCH: Weinheim, Germany, 2003.
49. Zheng, J.; Kang, Y.K.; Therien, M.J.; Beratan, D.N. Generalized Mulliken−Hush analysis of electronic coupling interactions in compressed π-Stacked porphyrin−bridge−quinone systems. *J. Am. Chem. Soc.* **2005**, *127*, 11303–11310. [CrossRef]
50. Ryu, K.Y.; Lee, S.Y.; Park, D.Y.; Kim, S.Y.; Kim, C. A novel colorimetric chemosensor for detection of Co^{2+} and S^{2-} in an aqueous environment. *Sens. Actuators B Chem.* **2017**, *242*, 792–800. [CrossRef]
51. Tang, L.; Zheng, Z.; Bian, Y. N-2-hydroxyethylpiperazine dangled 2,5-diphenyl-1,3,4-oxadiazole-based fluorescent sensor for selective relay recognition of Cu^{2+} and sulfide in water. *Luminescence* **2016**, *31*, 1456–1460. [CrossRef]
52. Wang, L.; Bing, Q.; Li, J.; Wang, G. A new "ON-OFF" fluorescent and colorimetric chemosensor based on 1,3,4-oxadiazole derivative for the detection of Cu^{2+} ions. *J. Photochem. Photobiol. A Chem.* **2018**, *360*, 86–94. [CrossRef]
53. Cao, S.; Pei, Z.; Xu, Y.; Zhang, R.; Pei, Y. Polytriazole bridged with 2,5-diphenyl-1,3,4-oxadiazole moieties a highly sensitive and selective fluorescence chemosensor for Ag^{+}. *RSC Adv.* **2015**, *545*, 888–45896. [CrossRef]
54. Tekuri, V.; Sahoo, S.K.; Trivedi, D.R. Hg^{2+} induced hydrolysis of thiazole amine based Schiff base Colorimetric and fluorogenic chemodosimeter for Hg^{2+} ions in an aqueous medium. *Spectrochim. Acta Part A Mol. Biomol.* **2019**, *218*, 19–26. [CrossRef]
55. Duan, J.; Ma, B.; Liu, F.; Zhang, S.; Wang, S.; Kong, Y.; Du, M.; Han, L.; Wang, J.; Sang, Y.; et al. Coordination ability determined transition metal ions substitution of Tb in Tb-Asp fluorescent nanocrystals and a facile ions-detection approach. *Nanoscale* **2018**, *10*, 7526–7535. [CrossRef]
56. Ipate, A.; Hamciuc, C.; Homocianu, M.; Musteata, V.E.; Nicolescu, A.; Bruma, M.; Belomoina, N. Highly fluorinated poly 1,3,4-oxadiazole-ethers structural, optical and dielectric characteristics. *J. Polym. Res.* **2015**, *22*, 95. [CrossRef]
57. Suppan, P. Excited-state dipole moments from absorption/fluorescence solvatochromic ratios. *Chem. Phys. Lett.* **1983**, *94*, 272–275. [CrossRef]
58. Bicerano, J. *Prediction of Polymer Properties*; Marcel Dekker: New York, NY, USA, 2000.
59. Lou, A.J.-T.; Marks, T.J. A twist on nonlinear optics understanding the unique response of π-twisted chromophores. *Acc. Chem. Res.* **2019**, *52*, 1428–1438. [CrossRef]
60. Erande, Y.; Kothavale, S.; Sreenath, M.C.; Chitrambalam, S.; Joe, I.H.; Sekar, N. Triphenylamine derived coumarin chalcones and their red emitting OBO difluoride complexes synthesis, photophysical and NLO property study. *Dye. Pigment.* **2018**, *148*, 474–491. [CrossRef]